

DEVICE TECHNOLOGY

Ratcheting quasi-ballistic electrons in silicon geometric diodes at room temperature

James P. Custer Jr.¹, Jeremy D. Low¹, David J. Hill¹, Taylor S. Teitworth¹, Joseph D. Christesen¹, Collin J. McKinney², James R. McBride³, Martin A. Brooke⁴, Scott C. Warren^{1,5}, James F. Cahoon^{1*}

Ratcheting effects play an important role in systems ranging from mechanical socket wrenches to biological motor proteins. The underlying principle is to convert a fluctuating, unbiased force into unidirectional motion. Here, we report the ratcheting of electrons at room temperature using a semiconductor nanowire with precisely engineered asymmetry. Modulation of the nanowire diameter creates a cylindrical sawtooth geometry with broken inversion symmetry on a nanometer-length scale. In a two-terminal device, this structure responded as a three-dimensional geometric diode that funnels electrons preferentially in one direction through specular reflection of quasi-ballistic electrons at the nanowire surface. The ratcheting effect causes charge rectification at frequencies exceeding 40 gigahertz, demonstrating the potential for applications such as high-speed data processing and long-wavelength energy harvesting.

Ratchets take various forms, from socket wrenches that convert mechanical action into rotation, to biological motor proteins that convert thermal fluctuations into transport (*1*). In general, ratchets convert an unbiased fluctuating force into unidirectional motion (*2*). A tilting ratchet (Fig. 1A), for instance, has a spatially periodic but asymmetric geometry or potential that converts an oscillating force into directed motion (*3*). Tilting ratchets have been realized for microscopic particle-based systems such as microfluidic beads (*4*); however, electron ratcheting effects, reported in only a handful of instances (*3, 5–7*), have remained a challenge because of the inherently short time and length scales of electron motion. Here, we report tilting ratchets for quasi-ballistic electrons using asymmetric diameter-modulated silicon nanowires (NWs). The NW ratchets conduct current preferentially in one direction and behave as high-frequency geometric diodes at room temperature, overcoming limitations of more conventional devices and enabling energy harvesting and signal processing technologies.

Like ratchets, conventional electrical diodes—which include two-terminal semiconductor p-n junctions and metal-semiconductor Schottky barriers—control the flow of electrons. However, they operate through a fundamentally different set of mechanisms, relying on capacitive depletion regions, band bending, and band offsets for their function. In a Schottky diode (Fig. 1B), electrical current flows in the

forward direction through thermionic emission of electrons over a voltage-dependent potential barrier, and current is blocked in the reverse direction by the Schottky barrier (*8*). Typical diodes can achieve direct current (dc) asymmetries, calculated as the magnitude of the ratio of forward-bias current, $I(+|V_{\text{app}}|)$, to reverse-bias current, $I(-|V_{\text{app}}|)$, at a given applied voltage (V_{app}), greater than 10^6 . However, because the operation of these diodes relies on a potential barrier, they possess a large capacitance. Thus, their ability to rectify alternating current (ac) at high frequencies is fundamentally limited by a resistance-capacitance (RC) time constant (*9*).

Geometric diodes are an alternative paradigm that takes advantage of noncentrosymmetric structures to induce current flow preferentially in one direction (*5, 10, 11*). A geometric diode (Fig. 1C) can be created by using a sawtooth geometry in which electrons undergo quasi-specular reflection at the boundaries of the structure, directing electrons through a constriction in the forward direction. In the reverse direction, electrons are reflected backward, blocking current. To function, the physical dimensions of a geometric diode must be comparable to the mean free path (MFP) of the majority carrier, allowing the devices to operate in the ballistic or quasi-ballistic regime, in which surface reflections dominate over other charge-carrier scattering mechanisms (*11*). These structures are theoretically limited not by RC time constants but by the inherent ballistic motion and flight time of charge carriers. Potential advantages include near zero-bias turn-on and ac operation into the terahertz regime (*9, 12*), unlocking applications that include high-speed signal processing or data transfer (*13, 14*) and long-wavelength energy harvesting (*15, 16*).

Four-terminal ballistic rectifiers operating at cryogenic temperatures (*17*) and room temperature (*18*) and quantum ratchets operating

at cryogenic temperatures (*3*) have been reported with two-dimensional electron gases. Rectifying devices have also been fabricated with graphene (*6, 19*), but two-terminal geometric diodes with large dc asymmetry (>5) at room temperature have yet to be realized. We demonstrate NW-based three-dimensional (3D) ballistic geometric diodes that exhibit dc asymmetries as high as 10^3 at room temperature and that ratchet electrons at ac frequencies exceeding 40 GHz. The two-terminal geometric diodes are composed of silicon (Si) NWs in which the diameter is modulated to produce a tapered, noncentrosymmetric sawtooth with cylindrical symmetry (Fig. 2A). Key geometric parameters include the outer wire diameter (D), constriction diameter (d), ratchet length (L), ratchet angle (θ), and constriction angle (φ). These single-crystal Si structures are fabricated by a bottom-up vapor-liquid-solid (VLS) growth process (*20*) using Au catalyst nanoparticles that dictate D .

To modulate diameter, the dopant precursor flow rate was rapidly varied during VLS

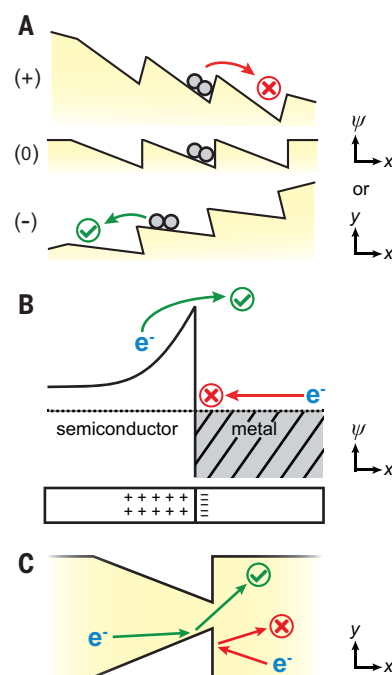


Fig. 1. Ratchets and diodes. (A) Schematic illustration of the tilting ratchet under positive, zero, and negative applied forces. Axes denote asymmetry in potential (ψ) or geometry (y) as a function of spatial position (x). (B) Band diagram of a Schottky-barrier diode (upper), showing metal on the right and the conduction band for an n-type semiconductor on the left. Dashed line represents the Fermi level. Lower schematic represents the depletion region, showing regions of positive and negative charge density at the semiconductor-metal interface. (C) Schematic illustration of a geometric diode in a sawtooth geometry showing specular reflection of electrons coming from the left and right.

¹Department of Chemistry, University of North Carolina at Chapel Hill, Chapel Hill, NC 27599, USA. ²Electronics Core Facility, University of North Carolina at Chapel Hill, Chapel Hill, NC 27599, USA. ³Vanderbilt Institute of Nanoscale Science and Engineering, Vanderbilt University, Nashville, TN 37235, USA. ⁴Department of Electrical and Computer Engineering, Duke University, Durham, NC 27708, USA. ⁵Department of Applied Physical Sciences, University of North Carolina at Chapel Hill, Chapel Hill, NC 27599, USA. *Corresponding author. Email: jfcahoon@unc.edu

growth to vary dopant concentration along the NW axis to yield abrupt and radially uniform profiles (21), as shown by scanning transmission electron microscopy elemental analysis for n-type NWs doped with phosphorus (fig. S1). Wet-chemical etching of the NWs yielded a diameter profile that is dependent on the encoded dopant profile (22, 23). For example, Fig. 2B displays scanning electron microscopy (SEM) images of two n-type NW segments that were etched under the same conditions but yielded different values of θ and d with the same D and L . The dopant and diameter profiles for the two segments (Fig. 2C) demonstrate that larger θ and lower d were synthetically encoded by using lower doping levels within the tapered region.

Thus, through control of catalyst diameter, etch conditions, and doping level, the fabrication process yielded direct structural tunability of the geometric parameters. The constriction angle φ is, however, limited from a more ideal value of 90° by the wet-etch process, yielding typical values of 30° to 60° . In addition, the bottom-up process allowed multiple geometric diodes to be encoded in series within a single NW (Fig. 2D). All ratchet geometries described herein used dopant profiles that produced nominally intrinsic Si at the constriction and had features on a scale comparable to the electron MFP in Si at room temperature, which we estimate to be ~ 10 to ~ 30 nm or more (see supplementary text section of the supplementary materials).

To probe the geometric diode behavior, n-type single-NW devices were fabricated (20), as shown by the representative SEM images in Fig. 2E. Four electrical contacts were defined per NW to ensure Ohmic contacts (fig. S2), and, except where noted, measurements were performed under vacuum directly after fabrication. The dc current-voltage (I - V) curves were collected using the polarity indicated in Fig. 2E, and room-temperature results for four NWs with θ ranging from 0° to 13° are shown in Fig. 3A. The NW with $\theta = 0^\circ$ showed a linear I - V response, whereas NWs with $\theta > 0^\circ$ showed increasingly nonlinear and diode-like I - V responses. The dc asymmetry of the devices progressively increased from unity to >10 for $|V_{\text{app}}| = 1$ V (Fig. 3A, inset). Results for >100 measured devices showed that the dc asymmetry exhibited the polarity indicated in the diode schematic in Fig. 2E with 100% yield. Moreover, devices with prolonged air exposure, for which native oxide had formed on the surface (fig. S3), yielded values $> 10^3$, as shown by the I - V curve and dc asymmetry data in Fig. 3B.

We modeled the diodes to understand the geometric dependence of the behavior. Finite-element (FE) electrostatic simulations (fig. S4), which have been shown to accurately describe NW p-n junctions (20, 24), demonstrated that

the degenerately doped n-type segments adjacent to the sawtooth geometry caused all potentials to drop across the sawtooth region and served as electron reservoirs that could inject electrons into the sawtooth region. However, the FE simulations did not reproduce the diode response of the devices because they did not account for the quasi-ballistic nature of electrons. Thus, we developed a simple analytical model (20, 25) to qualitatively capture these effects by describing the trajectories of single electrons within the sawtooth region (Fig. 3C, inset) assuming bal-

listic trajectories without phase coherence effects (see supplementary text) (11). The model integrates over trajectories that originate with a narrow angular distribution (accounting for the field-driven transport) within one MFP of the constriction, considering both direct transmission through the constriction and multiple specular reflections from the NW surface. It permits the calculation of transmission coefficients for passage through the constriction (11, 17), and we use the ratio (δ) of transmission coefficients in forward and reverse bias for qualitative comparison to the dc asymmetry measured by experiment (see supplementary text).

Figure 3C displays δ for different values of φ at a fixed L as a function of f -number (N) with $N = f/D$, where f is the effective focal length of the ratchet (Fig. 3C, inset) and $N = (2\tan(\theta))^{-1}$. For relatively large values of φ and N values above ~ 5 , the model predicted that as N decreased, δ increased. For N below ~ 5 , however, δ approached unity because d approached zero. The model also showed that δ depended strongly on the initial angular distribution, and substantially higher values could be achieved by varying this distribution (fig. S5). Moreover, for a fixed N , decreasing φ caused δ to decrease, because a smaller φ corresponded to an increasingly symmetric sawtooth structure.

Figure 3D displays experimental results correlating measured geometric structures with the I - V behavior. Champion devices for each value of N exhibited a trend of increasing dc asymmetry with decreasing N , in qualitative agreement with the trends for δ . As expected, there was no correlation between N and φ ; however, lower values of φ precluded a high dc asymmetry, in agreement with the trends for δ from the model. Images of three select devices (labeled 1 to 3), each with a dc asymmetry > 10 (Fig. 3D, inset) show the various geometries that produced high asymmetry values.

Because MFP substantially increases at lower temperatures (8, 26), we measured temperature-dependent I - V characteristics between 350 and 77 K (fig. S6). As temperature decreased, the dc asymmetry increased from 3.5 at 350 K to ~ 500 at 77 K, which is consistent with an increase in MFP. In addition, p-type NW devices were fabricated and exhibited a reversal of diode polarity, as expected because the majority carriers changed from electrons to holes (fig. S7). The low-temperature and p-type data thus further verified the quasi-ballistic mechanism of operation.

The champion room-temperature dc asymmetry (Fig. 3B), achieved with a stable surface oxide on n-type NWs after extended exposure to ambient conditions, yielded a value of ~ 1600 at $|V_{\text{app}}| = 1$ V with $\varphi = 46^\circ$ and $N = 5.4$. The higher asymmetry with surface oxide can be attributed to a smaller effective

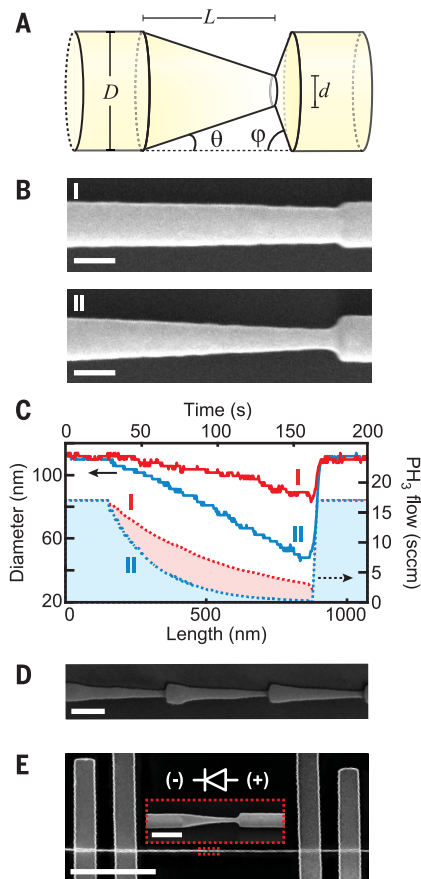
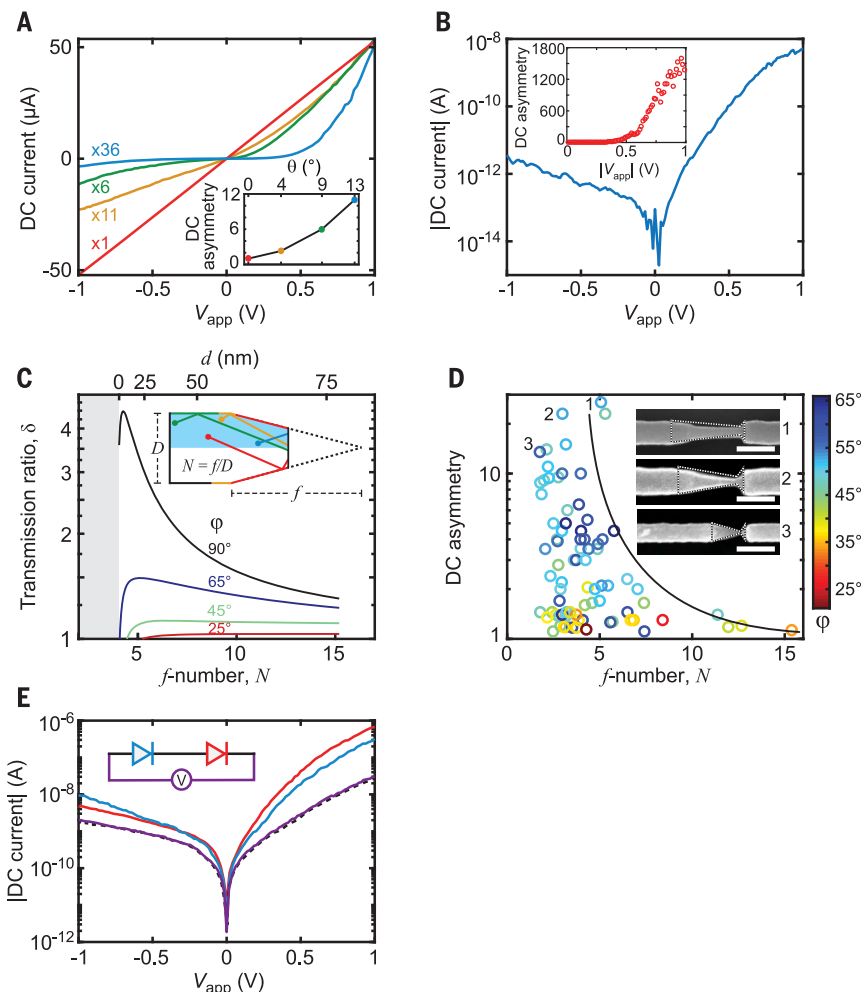


Fig. 2. Designing Si NW ratchets. (A) Design and geometric parameters for a two-terminal NW geometric diode with 3D morphology. (B) SEM images of two NW geometric diodes. Scale bars, 100 nm. (C) Diameter profiles (solid lines) and phosphine (PH_3) dopant precursor flow profiles (dashed lines) for the two geometric diodes, I (red) and II (blue), shown in (B). sccm, standard cubic centimeters per minute. (D) SEM image of a NW with three geometric diodes encoded in series. Scale bar, 200 nm. (E) SEM image of a single-NW device with two Ti/Pd electrical contacts on either side of the geometric diode. Scale bar, 5 μm . (Inset) Higher-magnification SEM image of the red boxed region and circuit-diagram representation of the geometric diode, showing the anode (+) and cathode (-). Scale bar, 250 nm.

Fig. 3. Two-terminal geometric diodes. (A) I - V curves measured from four separate single-NW devices with θ of 0° (red), 4° (orange), 9° (green), and 13° (blue). Current values for each device are scaled by the factors indicated. (Inset) The dc asymmetry at $|V_{\text{app}}| = 1$ V as a function of θ . (B) Semi-logarithmic I - V curve for a device with stable native oxide. (Inset) The dc asymmetry as a function of $|V_{\text{app}}|$. (C) δ calculated as a function of N (lower axis) with $D = 100$ nm and $L = 400$ nm, assuming φ of 90° (black), 65° (blue), 45° (green), and 25° (red), where MFP is $0.3D$. The d corresponding to values of N are shown on the upper axis. (Inset) Schematic illustration of the analytical model showing example trajectories of electrons originating within a set MFP of the constriction that successfully pass through the constriction. Colored trajectories denote qualitatively different pathways that involve either direct transmission (blue) or specular reflection (green, orange, and red) from the corresponding color-coded segments of the NW surface. The geometric parameters f and D that define N are also shown. (D) Experimental values of dc asymmetry at $|V_{\text{app}}| = 1$ V collected from 81 single-NW devices plotted as a function of N . Data points are color-coded according to the constriction angle φ . The black line is a guide to the eye. (Inset) SEM images of three high-asymmetry devices, labeled 1 to 3, overlaid with a diagram of their geometry. Scale bars, 200 nm. (E) Semi-logarithmic I - V curves for two diodes encoded in series within a single NW, showing the I - V response across both diodes (purple) and response of the individual diodes (red and blue). Dashed line represents the predicted response of the series-connected diodes based on the responses of individual diodes.



constriction and band bending that screened surface defects and improved specular reflection. Alternate surface passivation strategies, including aluminum oxide and thermal oxide, yielded similar results (fig. S8).

The bottom-up fabrication process also facilitated the series connection of multiple subunits within a single NW, as illustrated by the SEM image of geometric diodes in series in Fig. 2D. To test this design, I - V curves for two geometric diodes encoded in a single NW, measured separately and in series, are shown in Fig. 3E. When measured in series, the device exhibited the expected combined response from the two individual diodes because the nonballistic, degenerate n-type segments between the diodes acted as an ohmic connection between the two. Analogously, separate NWs can be wired in parallel, exhibiting the expected current summation (fig. S9). Together the results indicate that a combination of surface treatments and series or parallel connections can be used to create tunable I - V characteristics.

The quasi-ballistic operation of the geometric diodes enables electron ratcheting at high

ac frequencies, which manifests as rectification of an ac signal to produce a dc voltage (V_{dc}). The flight time of charge carriers through the quasi-ballistic region of the structure dictates the inherent response time, and for electrons at the Fermi velocity moving through the Si geometric diode, it is expected to exceed ~ 1 THz (see supplementary text). To test the frequency response of the diodes up to the instrumental limit of 40 GHz, the circuit shown diagrammatically in the inset of Fig. 4A was used to measure V_{dc} (20). Figure 4A shows the expected proportional increase of V_{dc} with power and verifies high-frequency electron ratcheting. Figure 4B shows V_{dc} as a function of frequency normalized by the separately measured transmitted power through a transmission line on the device chip (S_{21}) (20). This normalization partially accounted for frequency-dependent parasitic elements within the measurement system that alter the ac power applied to the device at each frequency (fig. S10). The quantity V_{dc}/S_{21} shows a relatively flat response from 100 MHz to 40 GHz, highlighting the broadband electron ratcheting effect in these diodes.

Because of their high-frequency response, the geometric diodes could be used for energy harvesting and signal processing applications. Figure 4C shows I - V curves of a geometric diode rectifying Wi-Fi signals (5.2 GHz) at varying powers. The I - V curves progressively shifted into quadrant II as ac power increased, corresponding to increasing power conversion and demonstrating the ability of the diodes to serve as long-wavelength energy harvesters in analogy to the operation of a solar cell (27). The geometric diodes could serve as the rectifying component of rectennas (15, 16, 28), harvesting background radiation for low-power consumption devices (29). Similarly, Fig. 4D shows the response of a geometric diode to a 20-GHz ac signal that was amplitude-modulated between -27 and -5 dBm to convey musical notes, producing clear V_{dc} levels for each signal amplitude. This example highlights the signal demodulation and processing capabilities of the geometric diodes. Together, Fig. 4, C and D, demonstrate that a single input signal could simultaneously provide data and be rectified into useable power (30). These demonstrations, combined with the ability to create

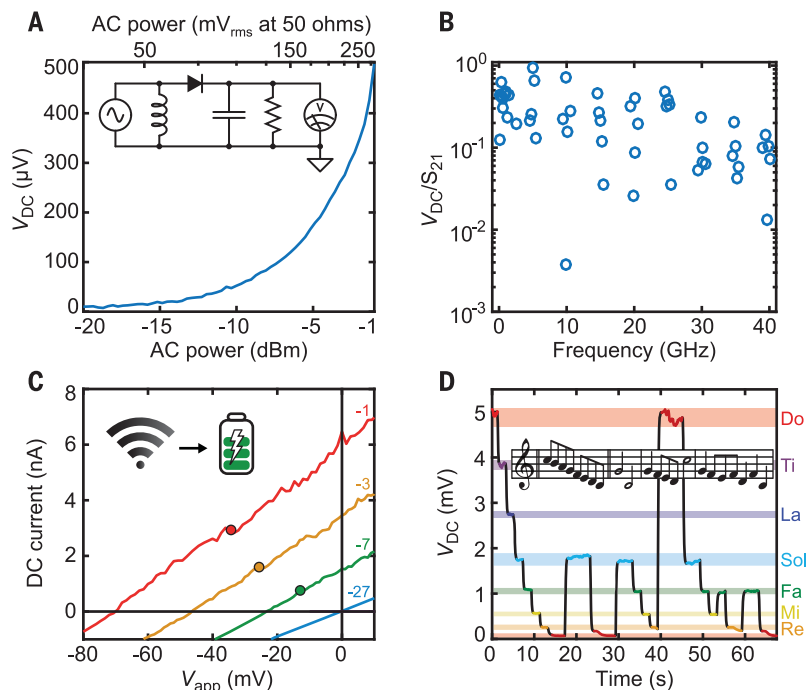


Fig. 4. High-frequency electron ratcheting.

(A) V_{dc} as a function of applied ac power at 40 GHz, with power displayed in units of decibel-milliwatts (dBm) (lower axis) or voltage across a 50-ohm load (upper axis). (Inset) Circuit diagram of the measurement setup. (B) V_{dc} normalized to S_{21} as a function of frequency for a single NW device. (C) I - V response of a geometric diode with 5.2-GHz ac applied at powers of -27 (blue), -7 (green), -3 (orange), and -1 dBm (red). Circles denote the maximum power points for each diode. (Inset) Schematic illustration of energy harvesting at Wi-Fi frequencies. (D) Demodulation of a 20-GHz square-wave amplitude modulated signal, corresponding to musical notes, by the geometric diode. The V_{dc} response time is limited not by the diode but by the measurement unit and integrating capacitor. Color-coding corresponds to the solfège shown on the right-hand axis. (Inset) Musical notation corresponding to the input signal.

parallel and series-connected custom diodes, highlight the potentially diverse application space for high-frequency electron ratchets operating at room temperature.

REFERENCES AND NOTES

- P. M. Hoffmann, *Rep. Prog. Phys.* **79**, 032601 (2016).
- B. Lau, O. Kedem, J. Schwabacher, D. Kwasnieski, E. A. Weiss, *Mater. Horiz.* **4**, 310–318 (2017).
- H. Linke *et al.*, *Science* **286**, 2314–2317 (1999).
- K. Louthback, J. Puchalla, R. H. Austin, J. C. Sturm, *Phys. Rev. Lett.* **102**, 045301 (2009).
- A. M. Song, *Appl. Phys. A Mater. Sci. Process.* **75**, 229–235 (2002).
- Z. X. Zhu, S. Joshi, G. Moddel, *IEEE J. Sel. Top. Quantum Electron.* **20**, 3801409 (2014).
- A. Lorke *et al.*, *Physica B* **249–251**, 312–316 (1998).
- S. M. Sze, K. K. Ng, *Physics of Semiconductor Devices* (John Wiley & Sons, ed. 3, 2007).
- D. M. Pozar, *Microwave Engineering* (Wiley, ed. 4, 2011).
- V. I. Belinicher, B. I. Sturman, *Sov. Phys. Usp.* **23**, 199–223 (1980).
- H. Linke, A. M. Song, in *Electron Transport in Quantum Dots*, J. P. Bird, Ed. (Springer, 2003), pp. 317–361.
- M. Tonouchi, *Nat. Photonics* **1**, 97–105 (2007).
- E. S. Kannan, I. Bisotto, J. C. Portal, T. J. Beck, L. Jalabert, *Appl. Phys. Lett.* **101**, 143504 (2012).
- B. Clerckx *et al.*, *IEEE J. Sel. Areas Comm.* **37**, 4–33 (2019).
- S. J. Byrnes, R. Blanchard, F. Capasso, *Proc. Natl. Acad. Sci. U.S.A.* **111**, 3927–3932 (2014).
- X. Zhang *et al.*, *Nature* **566**, 368–372 (2019).
- A. M. Song *et al.*, *Phys. Rev. Lett.* **80**, 3831–3834 (1998).
- A. M. Song *et al.*, *Appl. Phys. Lett.* **79**, 1357–1359 (2001).
- G. Auton *et al.*, *Nat. Commun.* **7**, 11670 (2016).
- See materials and methods in the supplementary materials.
- J. D. Christesen, C. W. Pinion, X. Zhang, J. R. McBride, J. F. Cahoon, *ACS Nano* **8**, 11790–11798 (2014).
- J. D. Christesen, C. W. Pinion, E. M. Grumstrup, J. M. Papanikolas, J. F. Cahoon, *Nano Lett.* **13**, 6281–6286 (2013).
- J. D. Christesen, C. W. Pinion, D. J. Hill, S. Kim, J. F. Cahoon, *J. Phys. Chem. Lett.* **7**, 685–692 (2016).
- J. D. Christesen *et al.*, *Nano Lett.* **12**, 6024–6029 (2012).
- P. Zhang, D. M. H. Hung, *J. Appl. Phys.* **115**, 204908 (2014).
- S. S. Li, W. R. Thurber, *Solid-State Electron.* **20**, 609–616 (1977).
- B. Lau, O. Kedem, M. Kodaimati, M. A. Ratner, E. A. Weiss, *Adv. Energy Mater.* **7**, 1701000 (2017).
- Z. Zhu, S. Joshi, S. Grover, G. Moddel, in *Rectenna Solar Cells*, G. Moddel, S. Grover, Eds. (Springer, 2013), pp. 209–227.
- X. Lu, P. Wang, D. Niyato, D. I. Kim, Z. Han, *IEEE Comm. Surv. and Tutor.* **17**, 757–789 (2015).
- T. D. Ponnimbaduge Perera, D. N. K. Jayakody, S. K. Sharma, S. Chatzinotas, J. Li, *IEEE Comm. Surv. and Tutor.* **20**, 264–302 (2018).

ACKNOWLEDGMENTS

Funding: This work was primarily supported by a Packard Fellowship for Science and Engineering to J.F.C. This work made use of instrumentation at the Chapel Hill Analytical and Nanofabrication Laboratory (CHANL), a member of the North Carolina Research Triangle Nanotechnology Network (RTNN), which is supported by the NSF (ECCS-1542015) as part of the National Nanotechnology Coordinated Infrastructure (NNCI). **Author contributions:** J.P.C., J.D.C., D.J.H., S.C.W., and J.F.C. designed experiments. J.P.C., J.D.L., and T.S.T. fabricated devices. J.P.C., J.D.L., and C.J.M. measured devices. C.J.M., J.D.L., and M.A.B. assisted with electrical measurement design. J.D.L. constructed the analytical model. J.P.C., J.D.C., D.J.H., and T.S.T. synthesized NWs. J.R.M. performed TEM analysis. J.P.C. and J.F.C. wrote the manuscript with input from all authors. J.F.C. supervised all aspects of the project. **Competing interests:** None declared. **Data and materials availability:** All data needed to evaluate the conclusions in the paper are present in the paper or the supplementary materials.

SUPPLEMENTARY MATERIALS

science.sciencemag.org/content/368/6487/177/suppl/DC1
Materials and Methods
Supplementary Text
Figs. S1 to S11
References (31–44)

26 July 2019; resubmitted 21 January 2020
Accepted 17 March 2020
10.1126/science.aay8663

Ratcheting quasi-ballistic electrons in silicon geometric diodes at room temperature

James P. Custer Jr., Jeremy D. Low, David J. Hill, Taylor S. Teitworth, Joseph D. Christesen, Collin J. McKinney, James R. McBride, Martin A. Brooke, Scott C. Warren and James F. Cahoon

Science **368** (6487), 177-180.
DOI: 10.1126/science.aay8663

Room-temperature electron ratchets

Conventional diodes rectify current flow by forming a junction between dissimilar conductors; a metal-semiconductor diode that forms a Schottky barrier is one example. In these devices, capacitance limits operating frequency. Custer *et al.* describe a diode made entirely of silicon that can rectify currents up to 40 gigahertz at room temperature. They fabricated silicon nanowires with a cylindrical sawtooth profile that act as ratchets, funneling current preferentially in one direction through specular reflection of quasi-ballistic electrons.

Science, this issue p. 177

ARTICLE TOOLS

<http://science.sciencemag.org/content/368/6487/177>

SUPPLEMENTARY MATERIALS

<http://science.sciencemag.org/content/suppl/2020/04/08/368.6487.177.DC1>

REFERENCES

This article cites 38 articles, 2 of which you can access for free
<http://science.sciencemag.org/content/368/6487/177#BIBL>

PERMISSIONS

<http://www.sciencemag.org/help/reprints-and-permissions>

Use of this article is subject to the [Terms of Service](#)

Science (print ISSN 0036-8075; online ISSN 1095-9203) is published by the American Association for the Advancement of Science, 1200 New York Avenue NW, Washington, DC 20005. The title *Science* is a registered trademark of AAAS.

Copyright © 2020 The Authors, some rights reserved; exclusive licensee American Association for the Advancement of Science. No claim to original U.S. Government Works